Article

Cell Chemical Biology

Targeting ribosomal G-quadruplexes with naphthalene-diimides as RNA polymerase I inhibitors for colorectal cancer treatment

Graphical abstract

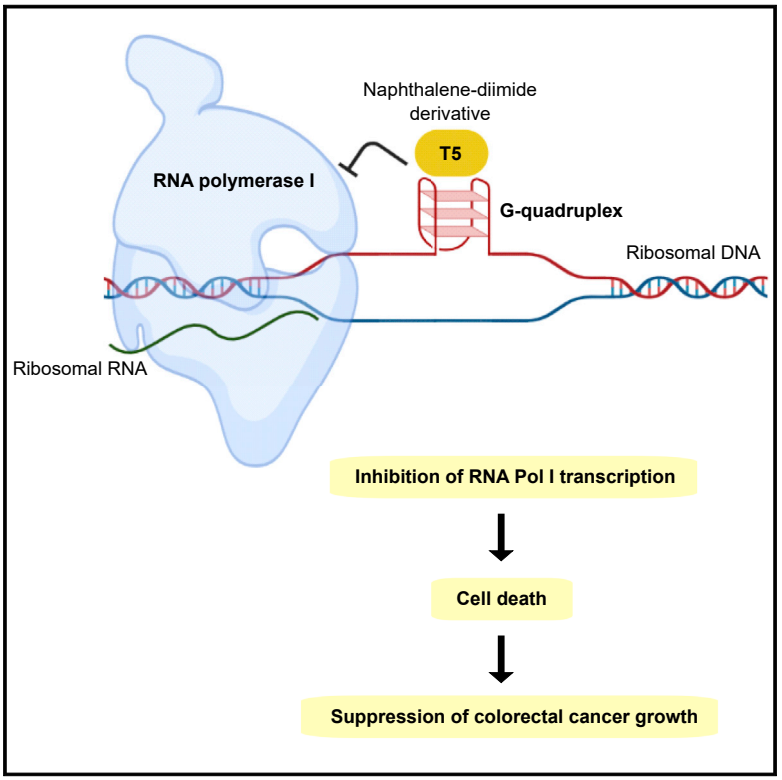

Highlights

- Evidence of naphthalene-diimides targeting ribosomal DNA G-quadruplexes

Authors

Victoria Sanchez-Martin, David A. Schneider, Matilde Ortiz-Gonzalez, ..., Carlos González, Miguel Soriano, Jose A. Garcia-Salcedo

Correspondence

jags@genyo.es

In brief

Sanchez-Martin et al. report a mode of action for naphthalene-diimides, a well-known class of G-quadruplexes ligands. Their work provides evidence of naphthalene-diimides targeting G-quadruplexes in ribosomal DNA, inducing a blockade of RNA polymerase I-mediated transcription and cell death. These compounds could be exploited in colorectal cancer treatment.

Sanchez-Martin et al., 2021, Cell Chemical Biology *28*, 1590–1601
November 18, 2021
https://doi.org/10.1016/j.chembiol.2021.05.021

CellPress

CellPress

Cell Chemical Biology

Article

Targeting ribosomal G-quadruplexes with naphthalene-diimides as RNA polymerase I inhibitors for colorectal cancer treatment

Victoria Sanchez-Martin,[1,2,3] David A. Schneider,[4] Matilde Ortiz-Gonzalez,[1,5] Ana Soriano-Lerma,[1,6] Angel Linde-Rodriguez,[1,2] Virginia Perez-Carrasco,[1,2] Jose Gutierrez-Fernandez,[2,7] Marta Cuadros,[1,3] Juan C. Morales,[8] Carlos González,[9] Miguel Soriano,[1,5,10] and Jose A. Garcia-Salcedo[1,2,10,11,*]

[1]GENYO. Centre for Genomics and Oncological Research: Pfizer/University of Granada/Andalusian Regional Government, Granada 18016, Spain

[2]Microbiology Unit, Biosanitary Research Institute IBS.Granada, University Hospital Virgen de las Nieves, Granada 18014, Spain

[3]Department of Biochemistry, Molecular Biology III and Immunology, University of Granada, Granada 18016, Spain

[4]Department of Biochemistry and Molecular Genetics, University of Alabama at Birmingham, Birmingham, AL 35294, USA

[5]Centre for Intensive Mediterranean Agrosystems and Agri-food Biotechnology (CIAIMBITAL), University of Almeria, Almeria 04001, Spain

[6]Department of Physiology, University of Granada, Granada 18011, Spain

[7]Department of Microbiology, University of Granada, Granada 18011, Spain

[8]Department of Biochemistry and Molecular Pharmacology, Instituto de Parasitología y Biomedicina López Neyra, CSIC, PTS Granada, Avda. del Conocimiento, 17, 18016 Armilla, Granada, Spain

[9]Instituto de Química Física "Rocasolano", CSIC, Madrid 28006, Spain

[10]These authors contributed equally

[11]Lead contact

*Correspondence: jags@genyo.es

https://doi.org/10.1016/j.chembiol.2021.05.021

SUMMARY

Guanine quadruplexes (G4s) are non-canonical nucleic acid structures commonly found in regulatory genomic regions. G4 targeting has emerged as a therapeutic approach in cancer. We have screened naphthalene-diimides (NDIs), a class of G4 ligands, in a cellular model of colorectal cancer (CRC). Here, we identify the leading compound T5 with a potent and selective inhibition of cell growth by high-affinity binding to G4s in ribosomal DNA, impairing RNA polymerase I (Pol I) elongation. Consequently, T5 induces a rapid inhibition of Pol I transcription, nucleolus disruption, proteasome-dependent Pol I catalytic subunit A degradation and autophagy. Moreover, we attribute the higher selectivity of carbohydrate-conjugated T5 for tumoral cells to its preferential uptake through the overexpressed glucose transporter 1. Finally, we succinctly demonstrate that T5 could be explored as a therapeutic agent in a patient cohort with CRC. Therefore, we report a mode of action for these NDIs involving ribosomal G4 targeting.

INTRODUCTION

Guanine quadruplexes (G4s) are non-B DNA structures derived from Hoogsteen hydrogen bonding of four guanines arranged within a planar quartet. Self-stacking of two or more G quartets generates a G4 structure that is further stabilized by monovalent cations and can display a wide variety of topologies (Hänsel-Hertsch et al., 2017). Computational predictions and direct G4 sequencing have identified more than 700,000 G4s in the human genome (Huppert and Balasubramanian, 2005; Todd et al., 2005; Chambers et al., 2015). More recently, 1,000–10,000 endogenous G4s have been detected in living cells through the use of G4-selective probes (Biffi et al., 2013; Hänsel-Hertsch et al., 2018). G4s are enriched in key regulatory sites, including promoters, gene bodies, and 5′ UTRs of highly transcribed genes, particularly those related to cancer, in somatic copy-number amplifications, ribosomal DNA, as well as telomeres (Hänsel-Hertsch et al., 2016). In these genomic locations, G4s are linked to fundamental biological processes, such as transcription, replication, genomic instability, and telomere maintenance (Hänsel-Hertsch et al., 2017). Thereby, G4 targeting is gaining relevance as a therapeutic approach to disrupt the aforementioned cellular processes (Balasubramanian et al., 2011). In fact, a series of well-known G4 stabilizers have been evaluated as an anticancer strategy (Neidle, 2017). Of particular note is CX-5461, which has recently entered clinical trials for patients with BRCA-deficient tumors (Xu et al., 2017).

To date, around 1,000 small molecules targeting G4 structures have been reported in the G-Quadruplex Ligands Database (Li et al., 2013). During the last decade, extensive research efforts have identified naphthalene-diimides (NDIs) as favored chemotypes for G4 binding because of their high target affinity, synthetic accessibility, and great potential for chemical variability (Cuenca et al., 2008; Arévalo-Ruiz et al., 2017; Răsădean et al., 2017). It is fully described that NDIs bind G4s at telomeres and oncogene

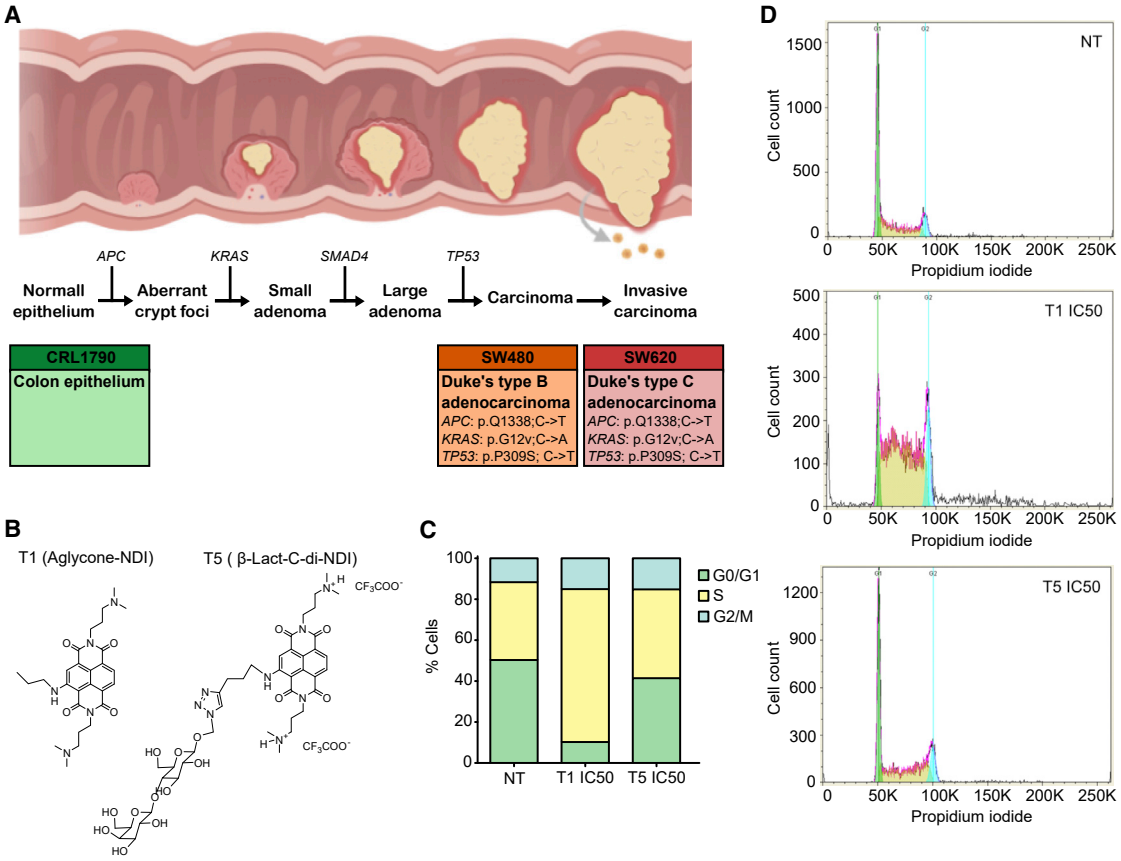

Figure 1. T1 and T5 show selective antitumor activity in a cellular model of colorectal carcinogenesis

(A) CRC model with the typical pattern of genetic aberrations according to the Cancer Cell Line Encyclopedia. Cell lines used for this study, CRL1790, SW480, and SW620, mimic different stages in colorectal carcinogenesis.

(B). Chemical structure of T1 (aglycone-NDI) and T5 (β-Lact-C-di-NDI) selected as antitumoral candidates in this study.

(C and D) Propidium iodide flow cytometry analysis of SW480 cells treated with DMSO (non-treated, NT) or treated with T1 IC_{50} or T5 IC_{50} for 24 h. (C) Stacked bar graph illustrating cell-cycle distribution. (D) Representative histograms are shown.

promoters with consequent antitumor activity (Pirota et al., 2019; Ahmed et al., 2020). Indeed, NDIs such as MM41 (Ohnmacht et al., 2015) and CM03 (Marchetti et al., 2018) have already shown promising results in cancer therapeutics.

Colorectal cancer (CRC) is the second most common cancer diagnosed in women and the third in men. It is a serious socio-medical problem causing almost 900,000 annual deaths worldwide (Dekker et al., 2019). In general, CRC formation begins with the transformation of a normal colorectal epithelium into a benign adenoma, which then progresses through the gradual accumulation of multiple genetic and epigenetic aberrations to an invasive and metastatic tumor (Nguyen and Duong, 2018). Conventional treatments for CRC, including surgery and radiochemotherapy, have had limited impact on cure rates and long-term survival (Kuipers et al., 2015) and, thus, screening programs of new drugs have gained momentum (Kuipers et al., 2015).

Therefore, the aim of this study was to investigate approaches based on G4 ligands for CRC treatment. We performed the screening of a previously reported NDI library (Arévalo-Ruiz et al., 2017; Zuffo et al., 2019) in a cellular model of CRC. We further elucidated the mode of action of the leading compound, T5, by multiple *in vitro* experiments, providing a molecular mechanism bridging the gap between G4 binding in rDNA and polymerase I (Pol I) inhibition. Moreover, we validated that the proposed selective inhibition of Pol I by T5 could be a promising therapeutic approach in a cohort of patients with CRC. Thereby, our study will lend further support to develop therapeutic strategies for successful CRC treatment.

RESULTS

Identification of two NDI derivatives (T1 and T5) with selective antitumor activity in a cellular model of CRC

To test the cytotoxic activity of a NDI library (Arévalo-Ruiz et al., 2017; Zuffo et al., 2019) at different stages in CRC, we established a cellular model to mimic colorectal carcinogenesis (Figure 1A). We used three different human cell lines: CRL1790 (colon epithelial cells) as non-tumoral stage, SW480 (Dukes' type B colorectal adenocarcinoma cells) representing the primary tumor stage, and SW620 (Dukes' type C colorectal adenocarcinoma derived from metastatic site cells) as the aggressive metastatic stage. To note, SW620 was established from a metastatic lymph node belonging to the same patient from whom the SW480 cell line was previously derived. According to the

Table 1. IC_{50} values and selectivity index for NDI derivatives in the cellular model of CRC

Treatment	Cell line	IC_{50} (μM)	Selectivity index
(T1) Aglycone-NDI 25	CRL1790	22.38 ± 2.64	–
(T1) Aglycone-NDI 25	SW480	6.81 ± 0.64	3.29
(T1) Aglycone-NDI 25	SW620	5.36 ± 0.61	4.18
(T2) α-Man-C2-di-NDI	CRL1790	>100	–
(T2) α-Man-C2-di-NDI	SW480	>100	1
(T2) α-Man-C2-di-NDI	SW620	37.15 ± 5.45	2.69
(T3) α-Man-C-di-NDI	CRL1790	23.93 ± 3.49	–
(T3) α-Man-C-di-NDI	SW480	20.18 ± 0.74	1.19
(T3) α-Man-C-di-NDI	SW620	11.64 ± 1.25	2.06
(T4) β-Lact-C2-tri-NDI	CRL1790	>100	–
(T4) β-Lact-C2-tri-NDI	SW480	>100	–
(T4) β-Lact-C2-tri-NDI	SW620	>100	–
(T5) β-Lact-C-di-NDI	CRL1790	50.46 ± 2.94	–
(T5) β-Lact-C-di-NDI	SW480	5.62 ± 0.57	8.98
(T5) β-Lact-C-di-NDI	SW620	7.94 ± 0.72	6.36
(T6) β-Malt-C-tri-NDI	CRL1790	>100	–
(T6) β-Malt-C-tri-NDI	SW480	>100	–
(T6) β-Malt-C-tri-NDI	SW620	>100	–
(T7) β-Man-TEG-di-NDI	CRL1790	>100	–
(T7) β-Man-TEG-di-NDI	SW480	70.79 ± 3.25	1.41
(T7) β-Man-TEG-di-NDI	SW620	53.33 ± 4.81	1.87

IC_{50} values represent NDI concentration inhibiting cell growth by 50% and are expressed as mean ± standard deviation. Selectivity index is the ratio of IC_{50} values in non-tumoral and cancer cell lines. Experiments were performed in biological triplicates. The nomenclature given for each NDI derivative corresponds to that used in a previously reported study (Zuffo et al., 2019).

Cancer Cell Line Encyclopedia database, both tumoral cell lines were characterized by the typical pattern of genetic aberrations defining CRC (*APC*, *K-RAS*, and *TP53* mutations).

Selection criteria for anticancer agents included cytotoxic potency and differential activity against tumoral versus normal cell lines (Hostettmann, 1991). Among seven NDI derivatives tested, only two met the selection criteria (Table 1). Aglycone-NDI (T1) and β-Lact-C-di-NDI (T5) inhibited SW480 and SW620 cell growth with half-maximal inhibitory concentration (IC_{50}) values lower than 30 μM and were much less cytotoxic to CRL1790, showing selectivity indexes greater than 2.0 (both compounds were over twice more cytotoxic to the tumor cells as compared with the normal cells). Cytotoxic activity, regardless of *TP53* mutational status, was confirmed in other CRC cell lines, such as HCT116 (*TP53* wild type) and HT29 (*TP53* pP309S; C- > T) (supplemental Figure S1). Based on these results, T1 and T5 were considered leading antitumor candidates, showing that T5 had a higher selectivity for tumoral cells. To note, T1 is an aglycone-NDI, while T5 is an NDI conjugated with a carbohydrate, lactose in particular (Figure 1B).

Next, we extended these findings by performing cell-cycle assays. Both NDIs triggered an S phase arrest, to a lower extent with T5, and a G2/M increase (Figure 1C). Propidium iodide cell-cycle analysis (Figure 1D) showed that T1/T5 IC_{50} treatments during 24 h were minimally toxic with only a <5% increase in the sub-G1 population. Therefore, both NDIs affected cell cycle and were considered for subsequent analysis.

T1 and T5 cause nucleolus disintegration, loss of Pol I catalytic subunit A, and autophagy

T1 and T5 derivatives belong to the NDI family, known to be G4 ligands. However, NDI binding to G4s in rDNA has not been previously studied. To explore this hypothesis, we performed an immunofluorescence of SW480 cells treated with T1/T5 IC_{50} for 24 h to determine the intracellular localization of nucleolar proteins indicative of nucleolus status (Hernandez-Verdun, 2006). Markedly, both derivatives caused segregation of nucleolar structures, including translocation of the granular component protein nucleolin to the nucleoplasm, segregation of fibrillarin to the nucleolar periphery caps and loss of Pol I catalytic subunit A (POLR1A) (Figure 2A). Zoom in of these images are shown in supplemental Figure S2. Therefore, T1 and T5 caused a remarkable nucleolar stress.

To confirm these alterations in POLR1A protein levels, we performed a western blot of SW480 cell lysates treated with T1/T5 IC_{50} for 3, 6, and 24 h. T1 and T5 markedly induced a POLR1A clearance (Figure 2B). Quantitatively, POLR1A was downregulated around 3, 10, and 40 times in cells treated for 3, 6, and 24 h, respectively (Figure 2C). We then checked whether such POLR1A degradation at 3 h was impaired after treatment with the proteasome inhibitor MG132 (10 μM, 6 h). We proved that inhibition of ubiquitination by MG132 rescued POLR1A degradation caused by T1 and T5 (Figure 2D). However, POLR1A clearance observed at the protein level was not associated with a decrease in POLR1A mRNA levels after treatment with T1/T5 IC_{50} for 3 h (Figure S3). Next, to explore the relationship between nucleolar stress and autophagy (Katagiri et al., 2015), we treated SW480 cells with T1/T5 IC_{50} for 24 h and assessed LC3 protein levels as an indicator of autophagy. Although T1 exerted a more potent effect, both NDIs led to the conversion of LC3-I to LC3-II, thus inducing autophagy (Figure 2E). We quantitatively confirmed that LC3-II production upon T1/T5 treatment for 24 h was significant (Figure 2F). Altogether, these results show that T1 and T5 induced proteasome-dependent POLR1A degradation, leading to cell death by autophagy.

T1 and T5 inhibit rRNA synthesis and cause POLR1A disassembly from rDNA prior to POLR1A degradation

Since disruption of the nucleolar structure is a cellular hallmark of rRNA transcription impairment (Hernandez-Verdun, 2006), we aimed to determine whether T1 and T5 affected cellular transcription by Pol I using qRT-PCR and considering the short-lived 5′ external transcribed spacer (5′ETS) of the pre-RNA (Figure 3A), whose abundance is generally reflective of the rRNA synthesis rate (Popov et al., 2013). We observed a drastic and significant decrease of 5′ETS transcripts (Figure 3B) in SW480 cells treated with T1/T5 IC_{50} for 3 h. To further assess the extent to which rRNA synthesis was inhibited by T1 and T5, we analyzed Pol I transcription in SW480 cells using both compounds at doses below their IC_{50} (0.5, 1, and 2.5 μM) for 3 h. Concentrations of 0.5 μM for T1 and 1 μM for T5 showed a 10- and 5-fold inhibition of rRNA synthesis, respectively (Figure 3C). In addition, we excluded that neither T1 0.5 μM nor T5 1 μM for 3 h had inhibitory effect on Pol II-driven transcription of G4-enriched genes through quantification of *BCL-2*, *C-MYB*, *C-MYC*, and *K-RAS* expression

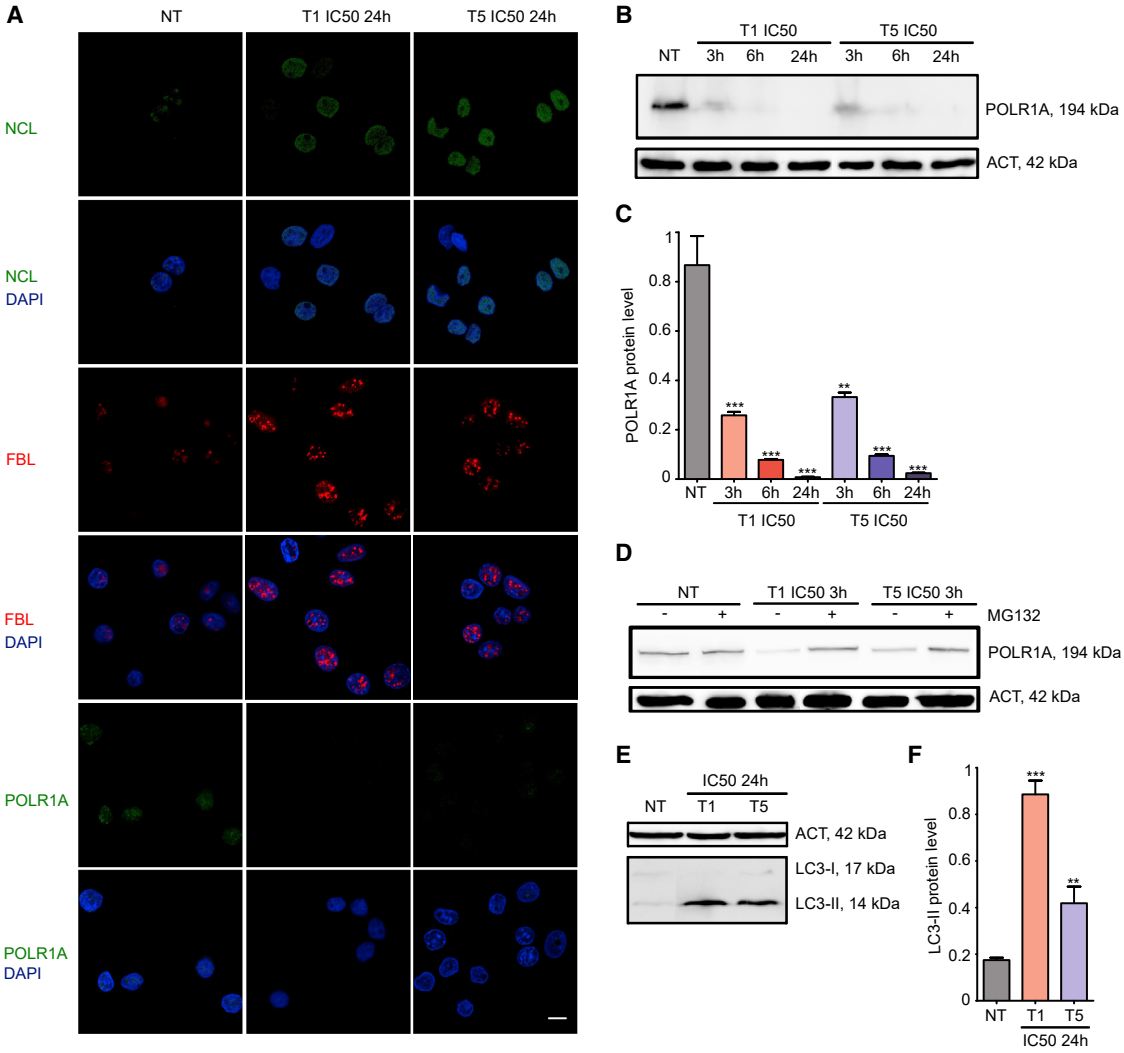

Figure 2. T1 and T5 induce nucleolus disintegration, proteasome-dependent POLR1A degradation, and autophagy

(A) SW480 cells were treated with DMSO (NT) or treated with T1 or T5 IC_{50} for 24 h and stained for nucleolin (NCL), fibrillarin (FBL), and POLR1A by immunofluorescence. Merged image with DAPI for DNA staining is shown below. Scale bar, 10 μm.

(B) Western blot analysis performed in SW480 cells after treatment with T1 or T5 IC_{50} for 3, 6, or 24 h, or treated with DMSO (NT) to determine protein levels of POLR1A and actin as housekeeping gene.

(C) Quantification of POLR1A protein levels normalized to actin data in (B).

(D) POLR1A and actin immunoblotting analysis of SW480 cells preincubated with the proteasome inhibitor MG132 (10 mM) for 6 h and subsequently treated with DMSO (NT) or treated with T1 or T5 IC_{50} for 3 h.

(E) Western blot analysis of SW480 cells treated with T1 or T5 IC_{50} for 24 h or DMSO (NT) to determine actin and LC3 (both LC3-I and LC3-II) protein levels as an autophagy marker. All western blot experiments were performed in biological triplicate.

(F) Quantification of LC3-II protein levels normalized to actin of data in (E).

levels by qRT-PCR (Figure S4). Therefore, a prominent inhibition of Pol I transcription was observed after NDI treatment for 3 h with an inhibitory concentration of 0.5 μM for T1 and 1 μM for T5.

Next, to analyze the kinetics of the cellular response to T1 and T5, we treated SW480 cells with T1/T5 at inhibitory concentrations for 0.5-, 1- and 3 h and measured rRNA synthesis. A significant decrease in 5′ETS transcript was observed after treatment, with a minimum inhibition at 30 min and a maximum inhibition at 3 h (Figure 3D). As rDNA transcription occurs via modulation of the assembly efficiency of Pol I transcription complex subunits on rDNA (Gorski et al., 2008), we tested whether T1 0.5 μM or T5 1 μM for 3 h could be altering POLR1A engagement with rDNA by POLR1A-chromatin immunoprecipitation and qPCR using primers for different regions of the rDNA gene body. As a consequence of T1 and T5 treatment, POLR1A association with rDNA was significantly affected throughout the rDNA gene (Figure 3E). Altogether, these results are consistent with a rapid kinetics regarding the inhibition of rRNA synthesis and a POLR1A disengagement from rDNA, suggesting the ribosomal locus as the main target of T1 and T5.

Our next aim was to assess the induction of POLR1A degradation at the inhibitory concentration (lower than IC_{50}). For this

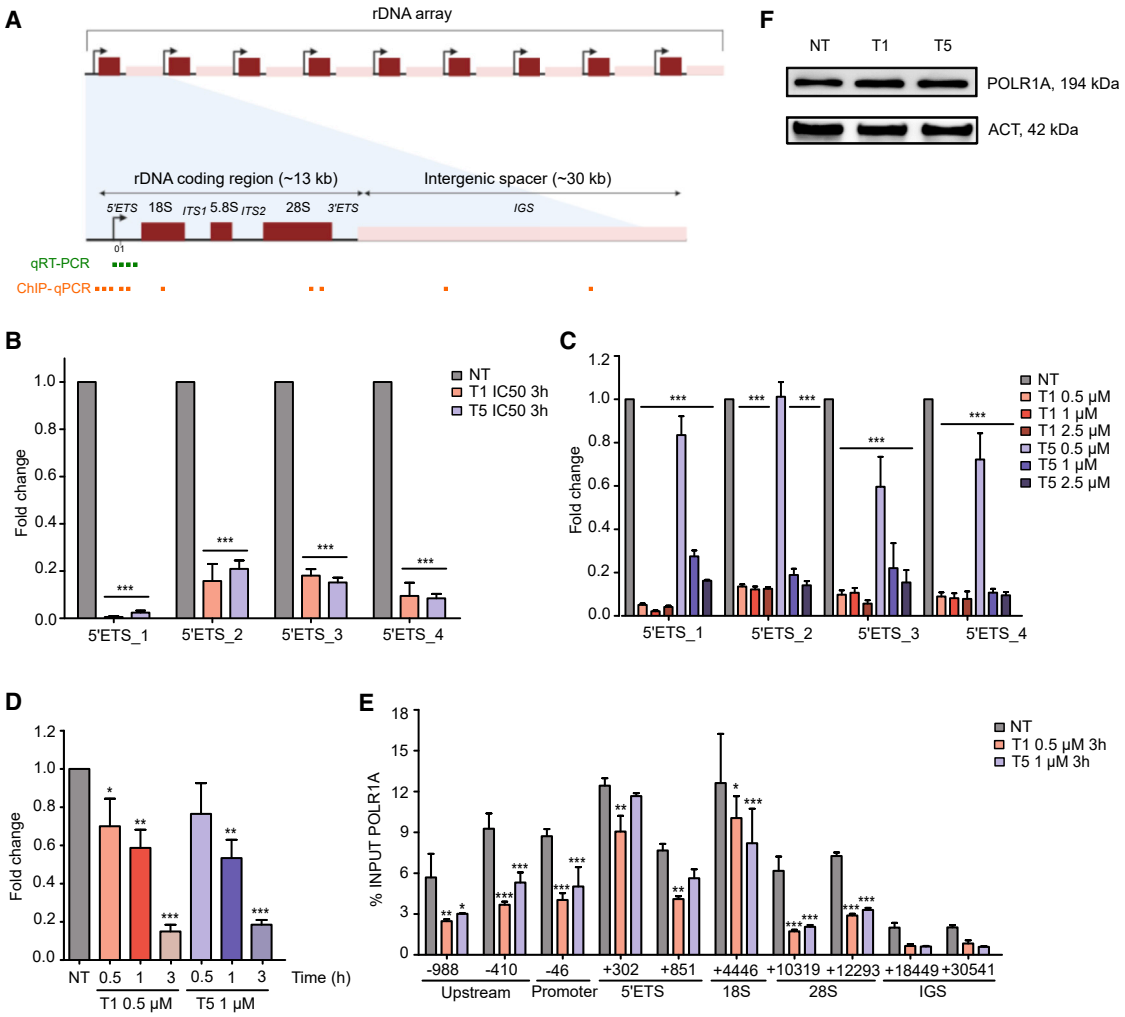

Figure 3. T1 and T5 rapidly induce inhibition of rRNA synthesis and POLR1A disengagement prior to POLR1A clearance

(A) Diagram of human tandem arrangement of rDNA repeated units, each containing an rRNA coding region (red) and an intergenic spacer (pink). Location of qRT-PCR and chromatin immunoprecipitation (ChIP)-qPCR primers used for this study is marked in green and orange, respectively.

(B) SW480 cells were treated with T1 or T5 IC_{50} for 3 h and rDNA transcription was analyzed by qRT-PCR using four primer sets for short-lived 5′ETS rRNA.

(C) rDNA transcription analysis (as in B) in SW480 cells treated with T1 or T5 at lower doses than IC_{50} (0.5, 1, and 2.5 μM) for 3 h.

(D) Kinetic analysis of rDNA transcription by qRT-PCR using 5′ETS_1 primers in SW480 cells treated with T1 0.5 μM or T5 1 μM for 0.5, 1, and 3 h.

(E) ChIP-qPCR analyses of POLR1A binding to rDNA in SW480 cells treated with DMSO (NT) or treated with T1 0.5 μM or T5 1 μM for 3 h. Primer locations and associated rDNA region paired are shown on the x axis.

(F) POLR1A and actin (housekeeping) protein abundance determined by western blot in SW480 cells treated either with T1 0.5 μM or T5 1 μM for 3 h. All experiments were performed in biological triplicate.

purpose, protein extracts of SW480 cells treated with T1 0.5 μM and T5 1 μM for 3 h were subjected to western blot analysis. Surprisingly, POLR1A protein was not degraded at these doses (Figure 3F). Thereupon, within 3 h after T1 0.5 μM and T5 1 μM treatment, the inhibition kinetics of rRNA synthesis and POLR1A disengagement from rDNA is faster than POLR1A clearance, which could be considered a downstream effect.

T5 possesses a tumor-selective effect depending partly on GLUT1 overexpression

We sought to identify if the inhibition of rRNA synthesis was maintained across our cellular model of CRC. CRL1790, SW480, and SW620 cells treated with T1 0.5 μM, T5 1 μM, or CX5461 1 μM (as a positive control for Pol I inhibition) for 3 h were subjected to Pol I transcription analysis (Figure 4A). As a result, T1 significantly inhibited rRNA synthesis in all cell lines to the same extent. Conversely, T5 showed a significant and selective effect for tumoral cell lines SW480 and SW620, while rRNA levels remained unchanged in CRL1790 non-tumoral cells. CX5461 was confirmed to act as a non-selective RNA Pol I inhibitor in all cell lines. Next, we investigated stabilization properties of G4s for T1 and T5 in a cellular environment. It was achieved by immunofluorescence with the G4-selective antibody BG4 in CRL1790, SW480, and SW620 cells after incubation with T1 0.5 μM or T5 1 μM for 3 h. T1 induced a notorious increase of nuclear BG4 signal in all cell lines, while this effect was only

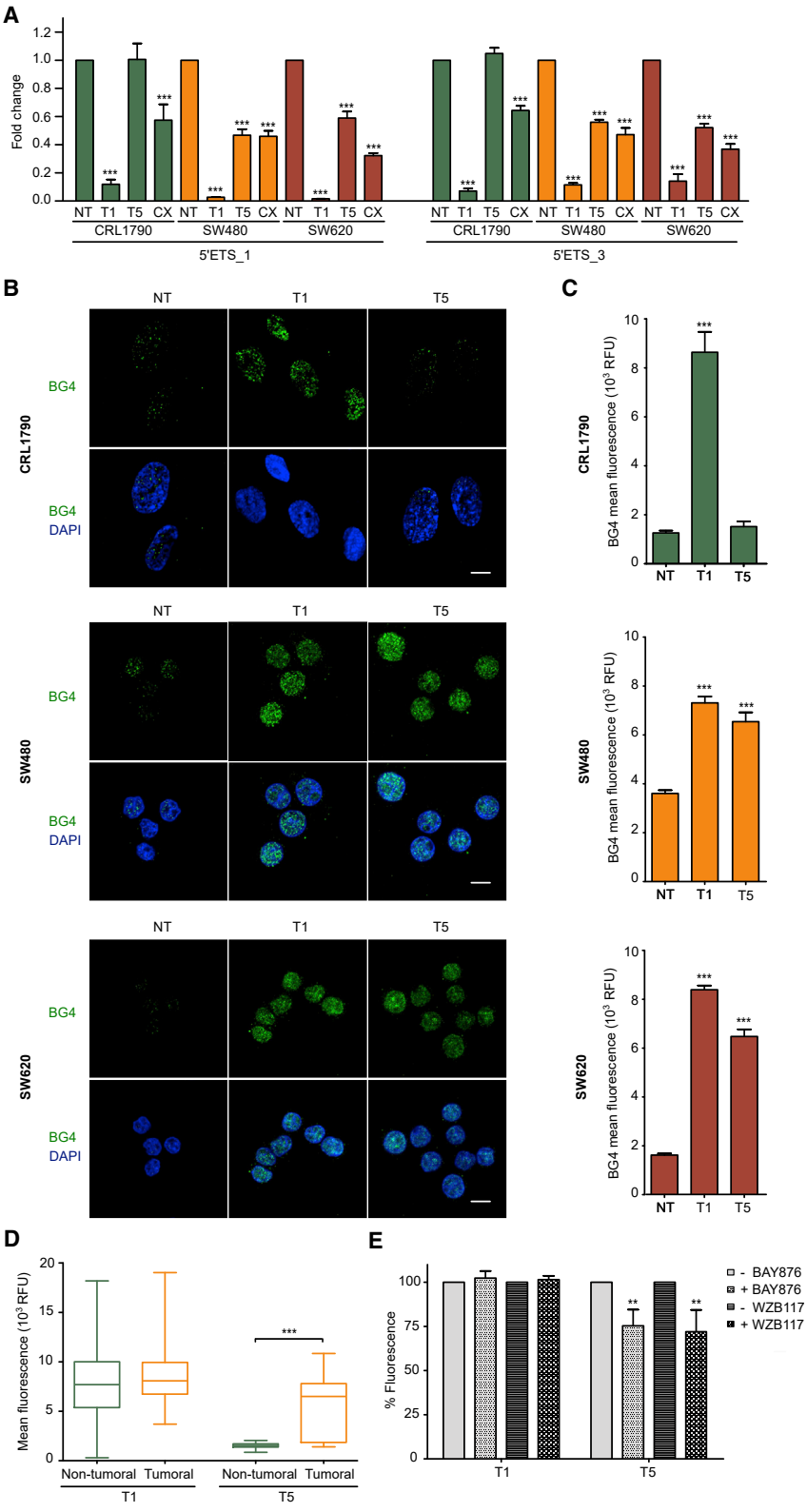

Figure 4. T5 possesses a tumor-selective effect depending partly on GLUT1 overexpression

(A) 5′ETS rRNA fold change across different cell lines in our cellular model of CRC determined in triplicate by qRT-PCR using 5′ETS_1 and 5′ETS_3 primers after T1 0.5 μM, T5 1 μM, or CX5461 1 μM treatment for 3 h or non-treated (NT).

(B) BG4 immunofluorescence images of CRL1790, SW480, and SW620 cells non-treated (NT) or treated with T1 0.5 μM or T5 1 μM for 3 h. Nuclei are colored blue by counterstaining with DAPI. Scale bars, 10 μm.

(C) Nuclear BG4 fluorescence level quantification from cells in (B) by Fiji analysis (N > 100).

(D) NDI nuclear uptake quantification from cells treated with T1 or T5 5 μM by fluorescence confocal microscopy and subsequent Fiji analysis (N > 50).

(E) T1 and T5 uptake quantification in SW480 cells in the absence or presence of BAY876 and WZB117 as GLUT1 inhibitors by fluorescence spectroscopy. Experiments were performed in triplicate.

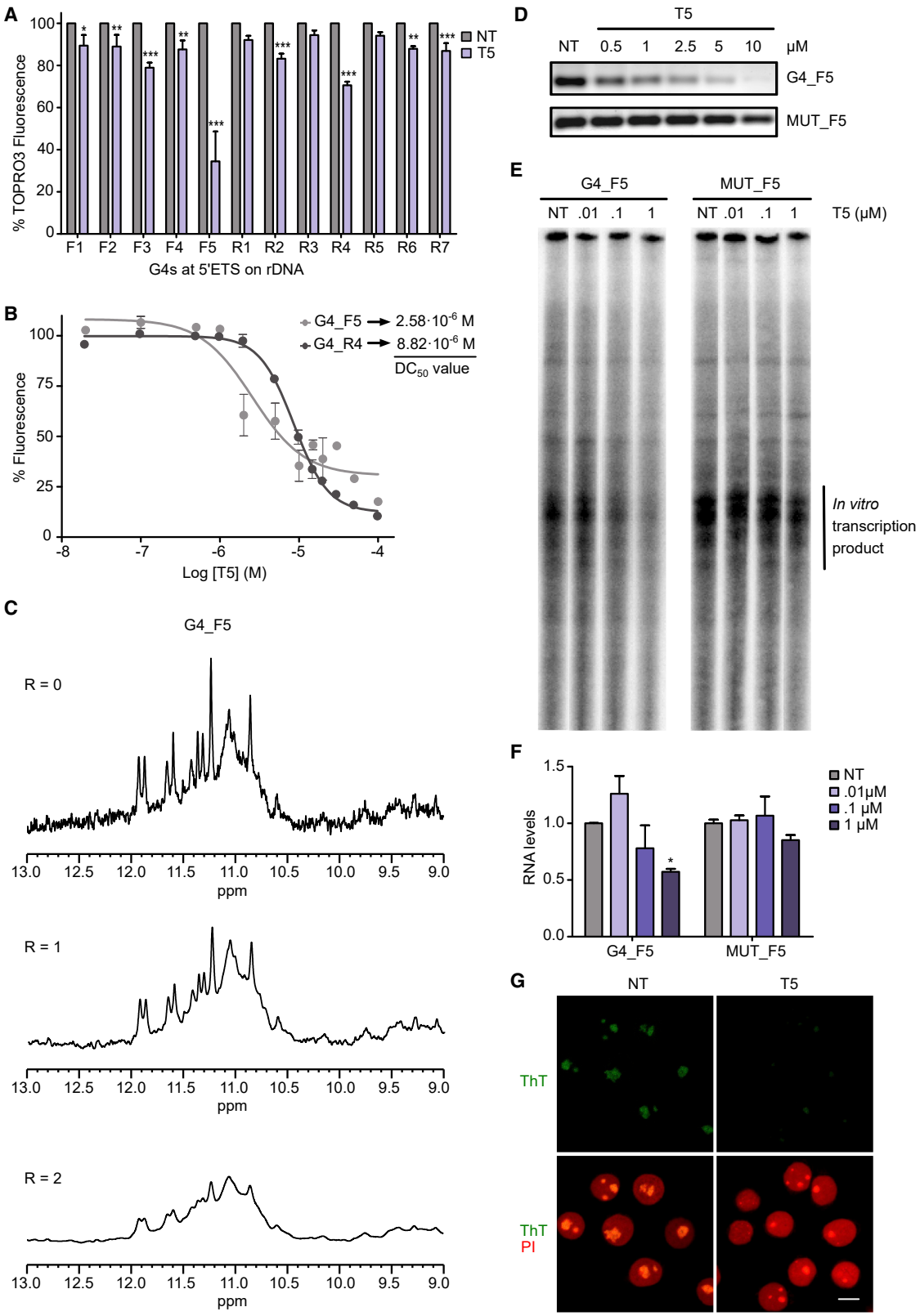

Figure 5. T5 exerts its function through binding to G4s in rDNA

(A) TOPRO3 FID assay using oligonucleotides from putative G4 sequences found in rDNA to determine the fluorescence percentage in the absence (NT) or presence of T5 5 µM. Experiments were performed in triplicate.

(legend continued on next page)

observed for tumoral SW480 and SW620 cells upon T5 treatment (Figure 4B). In accordance, BG4 mean fluorescence quantification (N > 100) rendered a significant increase after T1 and T5 treatment, indicating that these compounds strongly stabilized G4 structures, except for T5 in CRL1790 cells (where significant differences were not observed) (Figure 4C). Therefore, T5 offered the best therapeutic window with a predominant effect on tumoral cells.

NDIs are fluorescent molecules whose excitation and emission maxima take place at 595 and 661 nm, respectively (Arévalo-Ruiz et al., 2017). To further investigate the differences in tumoral selectivity between both compounds, we analyzed T1 and T5 uptake in our cellular model of CRC by fluorescence confocal microscopy and quantified the uptake profiles by measuring the nuclear fluorescence. No differences were found in cellular uptake between non-tumoral and tumoral cells for T1, while T5 showed a 4-fold greater entrance into tumoral cells (SW480) in relation to non-tumoral ones (Figure 4D). As mentioned before, T1 is an aglycone-NDI while T5 is a lactose-conjugated NDI, and such chemical differences could affect their uptake rates. Then, we hypothesized that T5 could be preferably translocated into cancer cells through glucose transporters (GLUTs). Since GLUT1 is frequently upregulated during oncogenesis (Ganapathy et al., 2009), we quantified the entrance of both NDI derivatives in SW480 cells in the presence of two different GLUT1 inhibitors: BAY876 (Siebeneicher et al., 2016) and WZB117 (Liu et al., 2012). T1 uptake was not affected after exposure to GLUT1 inhibitors. Notwithstanding, GLUT1 inhibition caused a significant decrease in T5 cellular uptake (Figure 4E). Therefore, T5 is preferably taken up by tumoral cells, at least in part, through GLUT1. However, additional uptake mechanisms associated with cancer cells must be involved. Due to its higher tumor selectivity, we further continued our study with T5.

T5 exerts its effect through binding to specific G4s in rDNA

Using the software QGRS mapper, we found 12 putative G4-forming sequences in the human ribosomal 5′ETS DNA region (Table S2). Inhibition of the rDNA transcription by T5 prompted us to examine whether T5 interacted with these G4-forming sequences by TOPRO3 fluoresecent intercalator displacement (FID) assay. Interestingly, T5 5 μM significantly exhibited a preferential binding to G4_F5 and G4_R4, decreasing the fluorescence percentage down to 34.5% and 70.6%, respectively (Figure 5A). Moreover, we performed FID titration assays using T5 from 0.02 to 100 μM with the selected G4_F5 and G4_R4 to quantify the concentration required to displace TOPRO3 from the DNA matrix by 50% (DC_{50} values) (Largy et al., 2011). To note, DC_{50} values were at micromolar range and T5 DC_{50} value for G4_F5 was significantly lower than for G4_R4 (Figure 5B). Therefore, we continued our study with G4_F5. Guanine imino signals between 10.5 and 12 ppm in the NMR spectrum clearly confirmed the formation of a G4 structure in G4_F5 (Figure 5C). Upon T5 addition, NMR signals changed due to interaction between T5 and the G4_F5. The general signal broadening suggested the formation of higher-order structures resulting from ligand-induced association of G4s. This behavior is common in many G4 ligands. To further assess the mode of action, we evaluated the ability of T5-stabilized G4_F5 sequence to stall a DNA polymerase by an *in vitro* DNA polymerase extension assay. As negative control, we used a mutant sequence incapable of G4 formation (MUT_F5). T5 demonstrated a selective and dose-dependent inhibition of PCR amplification for the wild-type G4_F5 (Figure 5D). In contrast, T5 had no effect on the DNA polymerase stalling in the mutant sequence. Overall, these results confirm that T5 exerts the inhibition of rRNA synthesis by a high-affinity binding to specific G4s in rDNA.

To test effects of T5 on Pol I transcription *in vitro*, a DNA template that fused the yeast rDNA promoter to the human rDNA sequence carrying the G4_F5 sequence or a mutated G4_F5 sequence were synthesized. These templates were included in fully reconstituted *in vitro* transcription assays using purified yeast components in multiple rounds (Keener et al., 1998; Bedwell et al., 2012). Promoter-dependent transcription of the linear templates yielded 756 nt runoff RNA products. RNA accumulation was significantly inhibited by addition of T5 in reactions, including the G4_F5 template (Figures 5E and 5F). Reactions using the mutant form of the G4 sequence were less affected by T5. The full-size image of the denaturing gel is included in Figure S5. Therefore, T5 directly inhibits transcription by RNA Pol I *in vitro*.

Next, we investigated in a cellular environment the stabilization properties of T5 in rDNA-associated G4s by a competition experiment in the presence of thioflavin T (ThT), a fluorescent light-up probe of ribosomal G4s in the nucleolus (Zhang et al., 2018). SW480 cells non-treated or treated with T5 1 μM for 3 h were subjected to ThT fluorescence confocal microscopy. In non-treated cells, ThT foci mainly accumulated in the nucleoli. In contrast, the ThT-stained foci sharply decreased upon treatment with T5, indicating that T5 displaced ThT from the nucleolar G4s (Figure 5G). These results further sustain that T5 exhibits a G4-binding pattern inside cells and mainly targets G4s in the nucleolar rDNA at physiological conditions.

T5 could be explored as a therapeutic agent for patients with CRC

Since POLR1A activity rate is proportional to cell proliferation (Pelletier et al., 2017), we postulated that POLR1A expression was increased along colorectal carcinogenesis to meet the increasing demands for protein synthesis and, thus, it could be

(B) FID titration assay with increasing concentrations of T5 to determine DC_{50} values in the selected putative G4s. Experiments were conducted in triplicate.
(C) Exchangeable proton region of the NMR spectra of G4_F5 with T5 at different R = [T5]/[DNA] ratios.
(D) PCR stop assay to determine the effect of T5 on the stabilization of the G4-forming candidate G4_F5 and mutant MUT_F5 with increasing T5 concentrations. Three independent reactions were conducted per concentration and representative lanes are displayed.
(E) Pol I *in vitro* transcription elongation assay of the yeast/human rDNA fusion template carrying the G4_F5 sequence and a mutated MUT_F5 sequence. Each reaction was performed at least four independent times and representative lanes are shown for display purposes.
(F) Quantification of RNA levels from *in vitro* transcription experiments in (E).
(G) Fluorescence confocal imaging of SW480 cells pre-stained with thioflavin T non-treated (NT) or treated with T5 1 μM for 3 h. Nuclei are colored in red by counterstaining with propidium iodide (PI). Scale bar, 10 μm.

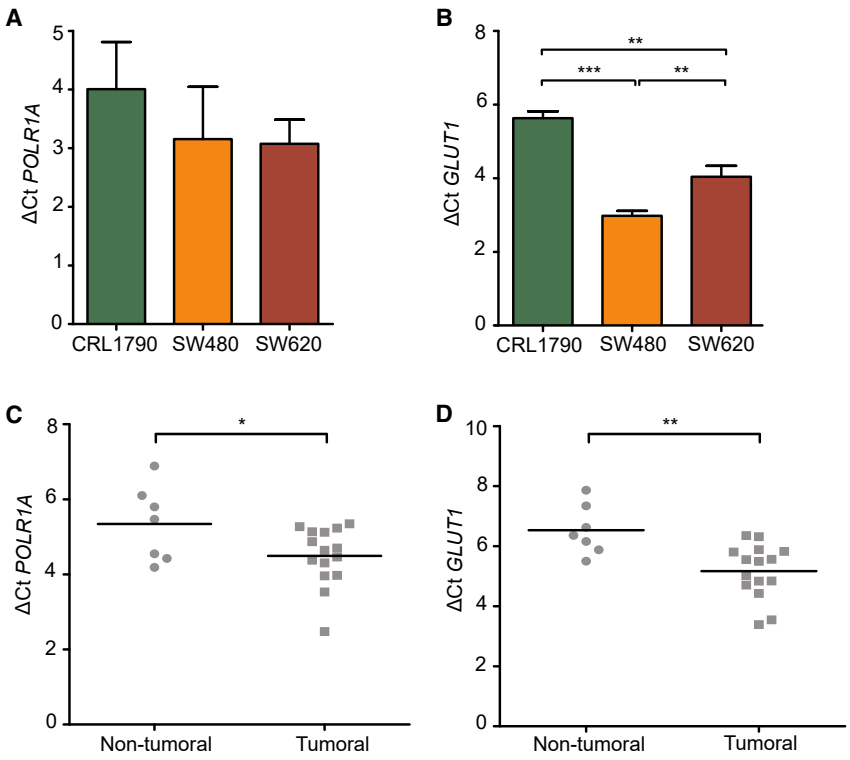

Figure 6. T5 could be explored as a therapeutic agent for CRC

(A) ΔCt results for POLR1A expression in the cellular model of CRC obtained by qRT-PCR.

(B) qRT-PCR results for ΔCt GLUT1 expression in the cellular model of CRC.

(C) ΔCt results for POLR1A expression in the cohort of patients with CRC, obtained by qRT-PCR.

(D) ΔCt GLUT1 expression levels considering the same patients in (C), determined by qRT-PCR. All qRT-PCR experiments were conducted in triplicate.

considered an attainable antitumor target in CRC. In particular, we determined *POLR1A* expression level in our cellular model of CRC by qRT-PCR. Ct is the threshold cycle of detection and ΔCt values show relative gene expression using actin as housekeeping gene. As expected, ΔCt *POLR1A* decreased in CRC meaning that *POLR1A* expression was higher in both tumoral cells, SW480 and SW620, versus CRL1790 normal cells (Figure 6A). We also appreciated that T1 and T5 IC_{50} values were correlated to *POLR1A* expression with a Pearson R value of 0.8669 ($p = 0.0254$). Overall, these results confirm that specific POLR1A inhibition by T1 and T5 represents a remarkable therapeutic opportunity in CRC. To further understand the selective mode of action of T5 in CRC, we aimed to analyze *GLUT1* expression levels in the cellular model of CRC. Both SW480 and SW620 cancer cells showed a significantly higher *GLUT1* expression (lower ΔCt *GLUT1*) in comparison with CRL1790 normal cells (Figure 6B). These results suggested that T5 is a more promising leading compound since its cellular uptake and inhibition of rRNA synthesis is partially restricted to tumoral cells owing to *GLUT1* overexpression.

Finally, we aimed to assess the translational potential of T5 in a patient cohort with CRC. To explore POLR1A inhibitors as a therapeutic strategy in CRC, *POLR1A* qRT-PCR analysis was performed in 15 CRC tumoral samples and 7 colorectal biopsies derived from non-tumoral adjacent tissue in patients with CRC. *POLR1A* mRNA expression was significantly upregulated (lower ΔCt *POLR1A*) in CRC compared with non-tumoral tissues (Figure 6C). Furthermore, since *GLUT1* overexpression would be exploitable for a targeted T5 treatment, we also analyzed *GLUT1* expression in patients with CRC by qRT-PCR. *GLUT1* expression level was significantly increased (lower ΔCt *GLUT1*) in tumoral compared with non-tumoral tissues (Figure 6D). *POLR1A* and *GLUT1* expression patterns observed in the patient cohort with CRC were further validated by a bioinformatic analysis from the Oncomine database (Figure S6). These findings reveal that POLR1A constitutes a clinically attainable target in CRC, while GLUT1 overexpression could be beneficial for a translational and targeted T5 treatment, evading undesirable side effects.

DISCUSSION

In this study, our main aim was to assess the potential therapeutic role of NDI G4 ligands in CRC, where only compounds interacting with the *K-RAS* promoter have been previously evaluated (Lavrado et al., 2015). We simulated colorectal carcinogenesis with a cellular model to identify the G4 ligands T1 and T5, which exhibited a potent and selective effect inhibiting cell growth *in vitro*. T1 and T5 belong to the NDI family, a class of small molecules capable of stabilizing G4s with high affinity (Cuenca et al., 2008). They are composed of a single naphthalene core that can be substituted with alternative side chains, from alkyls to amino acids (Răsădean et al., 2017) and carbohydrates (Arévalo-Ruiz et al., 2017), resulting in an extensive list of NDI derivatives. Interplay of different binding modes of NDIs to G4s with different topologies has been confirmed, with end-stacking always operative as the predominant binding event (Platella et al., 2020). Traditionally, NDIs have been considered to bind primarily to telomeric G4s and inhibit telomerase activity (Cuenca et al., 2008). More recent studies designated additional targets for G4 binding, including the promoters of *BCL-2* and *C-MYC* oncogenes (Pirota et al., 2019). However, this study reports the role of NDI derivatives on Pol I inhibition. In fact, to date most research has focused on *ex vivo* G4-binding assays with large amounts of NDIs. Very little is known about the primary role and mechanism of NDIs on tumoral cells at smaller concentration ranges. This work demonstrates that T1 and T5 NDI derivatives inhibit rRNA synthesis in a cellular context at concentrations even lower than IC_{50}. This gap between rRNA synthesis inhibition and its effect on cell proliferation may be due to the long half-life of human ribosomes (Boisvert et al., 2012).

In an attempt to study the precise manner in which T5 inhibits rDNA transcription, we identified specific rDNA sequences capable of forming stable G4s structures and mainly targeted

by T5 in physiological conditions. We propose a mechanism whereby binding of T5 to rDNA G4s causes the disengagement of POLR1A subunit and the consequent inhibition of transcription by Pol I. These rapid kinetic effects occur before the decrease in the abundance of POLR1A. Next, in response to the blockade of POLR1A near G4 sites, POLR1A is marked for proteasome-mediated clearance as a downstream effect. The *in vitro* transcription assays further support this model. Finally, T5 causes cell death by autophagy.

The above-mentioned activity is strikingly similar to other structurally distinct compounds described as first-in-kind Pol I inhibitors, such as BMH-21, CX-5461, and CX-3543. To note, redundancy in therapeutic strategies targeting Pol I is not only useful, but essential for clinical development. Notwithstanding, the proposed mechanism for T5 is a distinctive feature among the previously described Pol I inhibitors. Within them, BMH-21 has been suggested to intercalate within GC-rich regions in rDNA and promote degradation of POLR1A subunit (Wei et al., 2018). Alternatively, previous studies have also shown that CX-5461 exerts its effect through targeting the SL1 transcription factor, indispensable to recruit the Pol I preinitiation complex (Drygin et al., 2011). Conversely, CX-3543 disrupts nucleolin/rDNA G4 complexes in the nucleolus thereby inhibiting Pol I transcription (Drygin et al., 2009). In fact, a recent study proposed a role for both CX compounds as general G4 binders and remarked that both are mechanistically different from BMH-21, which revealed no detectable G4 binding (Xu et al., 2017). More recently, BMH-21 has been reported to bind to G4s in the *C-MYC* promoter (Musso et al., 2018). In this context, there is no strong evidence connecting Pol I inhibitors with the stabilization of rDNA G4s. At this point, it is worth noting the fact that T5 specifically targets G4s in rDNA backbone at the micromolar range, inducing a rapid inhibition of Pol I-mediated transcription as a consequence. In accordance with its preferential binding to rDNA G4s, T5 displaced ThT from nucleolar G4s in a cellular environment.

Selectivity is a major concern in cancer management to decrease adverse effects frequently attributed to classical cytotoxic drugs. Generally, two key processes contribute to a targeted therapy in cancer: exploiting unique features for tumor cells and enhancing drug uptake by malignant cells.

Firstly, Pol I is a highly active enzyme responsible for synthesizing rRNAs, the most abundant RNA species in the cell, constituting the rate-limiting step in ribosome biogenesis (Pelletier et al., 2017). Since cancer cells possess an increased ribosynthetic activity to meet their demands for increased protein synthesis, it is easily concluded that Pol I constitutes an emerging target in cancer therapeutics. Moreover, we show in this study that *POLR1A* is overexpressed both in tumoral and metastatic cell lines and in CRC tumor biopsies compared with the normal cell line and non-tumoral colon tissues, confirming that *POLR1A* expression rate is proportional to cell growth. These results are consistent with data showing deregulation of Pol I transcription in carcinogenesis (Drygin et al., 2010). In fact, POLR1A has been previously identified among other candidates as a biomarker in CRC (de Wit et al., 2014; Palma et al., 2014). Despite evidence, the clinical significance of Pol I had not been exploited before in CRC. On the other hand, we determine that *POLR1A* expression levels are inversely correlated with IC_{50} values in our cellular model. Searching for personalized medicine, these results could open up avenues to perform POLR1A expression analysis before treatment to potentially select the best responders to POLR1A inhibitors, such as T5.

Secondly, there is no denying that carbohydrate-NDI conjugation in T5 has contributed to promoting its selective entry into tumoral cells. It is widely established that tumor cells prioritize glucose uptake via increasing the number of GLUT receptors and coordinate an enhanced glucose entry with increased glycolysis (Warburg effect) to sustain a demanding and uncontrolled proliferation (Thorens and Mueckler, 2010). This study reveals that T5 is selectively taken up by cancer cells where GLUT1 seems to play a major role, although the influence of different GLUT isoforms still needs further investigations. Additional mechanisms could be also involved, including asialoglycoprotein receptors, which are overexpressed in tumoral tissues and specifically recognize galactose residues harbored in the lactose residue of T5 (Mu et al., 1994; Ma et al., 2015). The analysis of samples collected from patients with CRC and our cellular model demonstrate that *GLUT1* is overexpressed in cancer compared with non-tumoral specimens. In fact, GLUT1 is frequently upregulated during oncogenesis in many different types of tissues (Ganapathy et al., 2009), and GLUT1 overexpression has been previously considered as an unfavorable prognostic biomarker in patients with CRC (Yang et al., 2017). Altogether, these data highly reinforce that T5 takes advantage of the unique traits of cancer cells and elicits a potent and selective antitumor activity, while having minimal effect on non-malignant cells. Therefore, T5 would result in less genotoxic side effects than conventional therapy.

SIGNIFICANCE

This work describes a mode of action for naphthalene-diimides, a well-known class of G-quadruplex ligands. In previous studies, naphthalene-diimides have been considered to bind mainly to G-quadruplexes in telomeres and oncogenic promoters. However, our work provides evidence of naphthalene-diimide-targeting G-quadruplexes in ribosomal DNA. This action induces a blockade of RNA polymerase I-mediated transcription at low doses leading to inhibition of rRNA synthesis and cell death, which could be exploited in cancer treatment. Since tumoral cells possess an increased ribosynthetic activity, inhibition of RNA polymerase I represents an emerging target in cancer therapeutics. Moreover, we confirm that the carbohydrate-conjugated formulation of the selected naphthalene-diimide (T5) enhances its selectivity for tumoral cells partially due to overexpression of GLUT transporters in cancer.

STAR★METHODS

Detailed methods are provided in the online version of this paper and include the following:

- KEY RESOURCES TABLE
- RESOURCE AVAILABILITY
  - Lead contact
  - Materials availability

SUPPLEMENTAL INFORMATION

Supplemental information can be found online at https://doi.org/10.1016/j.chembiol.2021.05.021.

ACKNOWLEDGMENTS

We thank Juan Carlos Morales' laboratory (IPLN-CSIC, Granada, Spain) for kindly supplying GLUT inhibitors and NDI derivatives. We also thank Maria Jose Serrano's laboratory (Genyo, Granada, Spain) for supplying HCT116 and HT29 cell lines, and Pedro Real's group (Genyo, Granada, Spain) for providing us with MG132 reagent. We thank "Manuel Rico" NMR laboratory (LMR), a node of the Spanish Large-Scale National Facility (ICTS R-LRB) for performing NMR experiments. Finally, we gratefully acknowledge Javier Oliver (IPLN-CSIC, Granada, Spain) for supplying LC3 antibody and his valuable assistance. This work was supported by the European Commission (TARBRAINFECT to J.A.G.-S.) and the National Institutes of Health (GM084946 to D.A.S.). The Government of Spain granted with PhD fellowships FPU16/05822 to V.S.-M. and FPU17/05413 to A.S.-L. The University of Almeria granted with PhD fellowship to M.O.-G. Funding for open access charge: European Commission.

AUTHOR CONTRIBUTIONS

V.S.-M. performed the experiments and data analysis and wrote the manuscript. D.A.S. designed and performed the *in vitro* transcription experiments. M.C.C. supplied the patient samples and designed the respective experiments. C.G. designed and performed the NMR experiments. J.A.G.-S. and M.S. conceived the project, designed experiments, and edited the manuscript. All authors reviewed and edited the manuscript. All authors have given approval to the final version of the manuscript.

DECLARATION OF INTERESTS

The authors declare no competing interest.

Received: February 1, 2021
Revised: April 5, 2021
Accepted: May 27, 2021
Published: June 23, 2021; corrected online: December 16, 2021

REFERENCES

Ahmed, A.A., Angell, R., Oxenford, S., Worthington, J., Williams, N., Barton, N., Fowler, T.G., O'Flynn, D.E., Sunose, M., McConville, M., et al. (2020). Asymmetrically substituted quadruplex-binding naphthalene diimide showing potent activity in pancreatic cancer models. ACS Med. Chem. Lett. *11*, 1634–1644. https://doi.org/10.1021/acsmedchemlett.0c00317.

Arévalo-Ruiz, M., Doria, F., Belmonte-Reche, E., DeRache, A., Campos-Salinas, J., Lucas, R., Falomir, E., Carda, M., Pérez-Victoria, J.M., Mergny, J.L., et al. (2017). Synthesis, binding properties, and differences in cell uptake of G-quadruplex ligands based on carbohydrate naphthalene diimide conjugates. Chem. A Eur. J. *23*, 2157–2164. https://doi.org/10.1002/chem.201604886.

Balasubramanian, S., Hurley, L.H., and Neidle, S. (2011). 'Targeting G-quadruplexes in gene promoters: a novel anticancer strategy?'. Nat. Rev. Drug Discov. *10*, 261–275. https://doi.org/10.1038/nrd3428.

Bedwell, G.J., Appling, F.D., Anderson, S.J., and Schneider, D.a. (2012). Efficient transcription by RNA polymerase I using recombinant core factor. Gene *492*, 94–99. https://doi.org/10.1016/j.gene.2011.10.049.

Biffi, G., Tannahill, D., McCafferty, J., and Balasubramanian, S. (2013). Quantitative visualization of DNA G-quadruplex structures in human cells. Nat. Chem. *5*, 182–186. https://doi.org/10.1038/nchem.1548.

Boisvert, F.M., Ahmad, Y., Gierliński, M., Charrière, F., Lamont, D., Scott, M., Barton, G., and Lamond, A.I. (2012). A quantitative spatial proteomics analysis of proteome turnover in human cells. Mol. Cell. Proteomics *11*, 1–15. https://doi.org/10.1074/mcp.M111.011429.

Chambers, V.S., Marsico, G., Boutell, J.M., Di Antonio, M., Smith, G.P., and Balasubramanian, S. (2015). High-throughput sequencing of DNA G-quadruplex structures in the human genome. Nat. Biotechnol. *33*, 877–881. https://doi.org/10.1038/nbt.3295.

de Wit, M., Kant, H., Piersma, S.R., Pham, T.V., Mongera, S., van Berkel, M.P.A., Boven, E., Pontén, F., Meijer, G.A., Jimenez, C.R., et al. (2014). Colorectal cancer candidate biomarkers identified by tissue secretome proteome profiling. J. Proteomics *99*, 26–39. https://doi.org/10.1016/j.jprot.2014.01.001.

Dekker, E., Tanis, P.J., Vleugels, J.L.A., Kasi, P.M., and Wallace, M.B. (2019). Colorectal cancer. Lancet *394*, 1467–1480. https://doi.org/10.1016/S0140-6736(19)32319-0.

Drygin, D., Lin, A., Bliesath, J., Ho, C.B., O'Brien, S.E., Proffitt, C., Omori, M., Haddach, M., Schwaebe, M.K., Siddiqui-Jain, A., et al. (2011). Targeting RNA polymerase I with an oral small molecule CX-5461 inhibits ribosomal RNA synthesis and solid tumor growth. Cancer Res. *71*, 1418–1430. https://doi.org/10.1158/0008-5472.CAN-10-1728.

Drygin, D., Rice, W.G., and Grummt, I. (2010). The RNA polymerase I transcription machinery: an emerging target for the treatment of cancer. Annu. Rev. Pharmacol. Toxicol. *50*, 131–156. https://doi.org/10.1146/annurev.pharmtox.010909.105844.

Drygin, D., Siddiqui-Jain, A., O'Brien, S., Schwaebe, M., Lin, A., Bliesath, J., Ho, C.B., Proffitt, C., Trent, K., Whitten, J.P., et al. (2009). Anticancer activity of CX-3543: a direct inhibitor of rRNA biogenesis. Cancer Res. *69*, 7653–7661. https://doi.org/10.1158/0008-5472.CAN-09-1304.

Ganapathy, V., Thangaraju, M., and Prasad, P.D. (2009). Nutrient transporters in cancer: relevance to Warburg hypothesis and beyond. Pharmacol. Ther. *121*, 29–40. https://doi.org/10.1016/j.pharmthera.2008.09.005.

Gorski, S.A., Snyder, S.K., John, S., Grummt, I., and Misteli, T. (2008). Modulation of RNA polymerase assembly dynamics in transcriptional regulation. Mol. Cell *30*, 486–497. https://doi.org/10.1016/j.molcel.2008.04.021.

Hänsel-Hertsch, R., Beraldi, D., Lensing, S.V., Marsico, G., Zyner, K., Parry, A., Di Antonio, M., Pike, J., Kimura, H., Narita, M., et al. (2016). G-quadruplex structures mark human regulatory chromatin. Nat. Genet. *48*, 1267–1272. https://doi.org/10.1038/ng.3662.

Hänsel-Hertsch, R., Di Antonio, M., and Balasubramanian, S. (2017). DNA G-quadruplexes in the human genome: detection, functions and therapeutic potential. Nat. Rev. Mol. Cell Biol. *18*, 279–284. https://doi.org/10.1038/nrm.2017.3.

Hänsel-Hertsch, R., Spiegel, J., Marsico, G., Tannahill, D., and Balasubramanian, S. (2018). Genome-wide mapping of endogenous G-

quadruplex DNA structures by chromatin immunoprecipitation and high-throughput sequencing. Nat. Protoc. *13*, 551–564. https://doi.org/10.1038/nprot.2017.150.

Hernandez-Verdun, D. (2006). Nucleolus: from structure to dynamics. Histochem. Cell Biol. *125*, 127–137. https://doi.org/10.1007/s00418-005-0046-4.

Hostettmann, K. (1991). Assays for bioactivity. Method in plant biochemistry. New Phytol. 474.

Huppert, J.L., and Balasubramanian, S. (2005). Prevalence of quadruplexes in the human genome. Nucleic Acids Res. *33*, 2908–2916. https://doi.org/10.1093/nar/gki609.

Katagiri, N., Kuroda, T., Kishimoto, H., Hayashi, Y., Kumazawa, T., and Kimura, K. (2015). The nucleolar protein nucleophosmin is essential for autophagy induced by inhibiting Pol I transcription. Sci. Rep. *5*, 1–9. https://doi.org/10.1038/srep08903.

Keener, J., Josaitis, C.A., Dodd, J.A., and Nomura, M. (1998). Reconstitution of yeast RNA polymerase I transcription in vitro from purified components: TATA-binding protein is not required for basal transcription. J. Biol. Chem. *273*, 33795–33802. https://doi.org/10.1074/jbc.273.50.33795.

Kuipers, E.J., Grady, W.M., Lieberman, D., Seufferlein, T., Sung, J.J., Boelens, P.G., van de Velde, C.J.H., and Watanabe, T. (2015). Colorectal cancer. Nat. Rev. Dis. Primers *1*, 1–25. https://doi.org/10.1038/nrdp.2015.65.

Largy, E., Hamon, F., and Teulade-Fichou, M.P. (2011). Development of a high-throughput G4-FID assay for screening and evaluation of small molecules binding quadruplex nucleic acid structures. Anal. Bioanal. Chem. *400*, 3419–3427. https://doi.org/10.1007/s00216-011-5018-z.

Lavrado, J., Brito, H., Borralho, P.M., Ohnmacht, S.A., Kim, N., Leitão, C., Pisco, S., Gunaratnam, M., Rodrigues, C.M.P., Moreira, R., et al. (2015). KRAS oncogene repression in colon cancer cell lines by G-quadruplex binding indolo[3,2-c]quinolines. Sci. Rep. *5*, 1–10. https://doi.org/10.1038/srep09696.

Li, Q., Xiang, J., Yang, Q., Sun, H., Guan, A., and Tang, Y. (2013). G4LDB: a database for discovering and studying G-quadruplex ligands. Nucleic Acids Res. *41*, 1115–1123. https://doi.org/10.1093/nar/gks1101.

Liu, Y., Cao, Y., Zhang, W., Bergmeier, S., Qian, Y., Akbar, H., Colvin, R., Ding, J., Tong, L., Wu, S., et al. (2012). A small-molecule inhibitor of glucose transporter 1 downregulates glycolysis, induces cell-cycle arrest, and inhibits cancer cell growth in vitro and in vivo. Mol. Cancer Ther. *11*, 1672–1682. https://doi.org/10.1158/1535-7163.MCT-12-0131.

Ma, Y., Chen, H., Su, S., Wang, T., Zhang, C., Fida, G., Cui, S., Zhao, J., and Gu, Y. (2015). Galactose as broad ligand for multiple tumor imaging and therapy. J. Cancer *6*, 658–670. https://doi.org/10.7150/jca.11647.

Marchetti, C., Zyner, K.G., Ohnmacht, S.A., Robson, M., Haider, S.M., Morton, J.P., Marsico, G., Vo, T., Laughlin-Toth, S., Ahmed, A.A., et al. (2018). Targeting multiple effector pathways in pancreatic ductal adenocarcinoma with a G-quadruplex-binding small molecule. J. Med. Chem. *61*, 2500–2517. https://doi.org/10.1021/acs.jmedchem.7b01781.

Mu, J.Z., Fallon, R.J., Swanson, P.E., Carroll, S.B., Danaher, M., and Alpers, D.H. (1994). Expression of an endogenous asialoglycoprotein receptor in a human intestinal epithelial cell line, Caco-2. Biochim. Biophys. Acta *1222*, 483–491. https://doi.org/10.1016/0167-4889(94)90058-2.

Musso, L., Mazzini, S., Rossini, A., Castagnoli, L., Scaglioni, L., Artali, R., Di Nicola, M., Zunino, F., and Dallavalle, S. (2018). c-MYC G-quadruplex binding by the RNA polymerase I inhibitor BMH-21 and analogues revealed by a combined NMR and biochemical Approach. Biochim. Biophys. Acta *1862*, 615–629. https://doi.org/10.1016/j.bbagen.2017.12.002.

Neidle, S. (2017). Quadruplex nucleic acids as targets for anticancer therapeutics. Nat. Rev. Chem. *1*, 1–10. https://doi.org/10.1038/s41570-017-0041.

Nguyen, H.T., and Duong, H.Q. (2018). The molecular characteristics of colorectal cancer: implications for diagnosis and therapy (review). Oncol. Lett. *16*, 9–18. https://doi.org/10.3892/ol.2018.8679.

Ohnmacht, S.A., Marchetti, C., Gunaratnam, M., Besser, R.J., Haider, S.M., Di Vita, G., Lowe, H.L., Mellinas-Gomez, M., Diocou, S., Robson, M., et al. (2015). A G-quadruplex-binding compound showing anti-tumour activity in an in vivo model for pancreatic cancer. Sci. Rep. *5*, 1–11. https://doi.org/10.1038/srep11385.

Palma, P., Cano, C., Conde-Muiño, R., Comino, A., Bueno, P., Ferrón, J.A., and Cuadros, M. (2014). 'Expression profiling of rectal tumors defines response to neoadjuvant treatment related genes. PLoS One *9*, e112189. Edited by S. Wölfl. https://doi.org/10.1371/journal.pone.0112189.

Pelletier, J., Thomas, G., and Volarevic, S. (2017). Ribosome biogenesis in cancer: players and therapeutic avenues. Nat. Rev. Cancer *18*, 51–63. https://doi.org/10.1038/nrc.2017.104.

Pirota, V., Nadai, M., Doria, F., and Richter, S.N. (2019). Naphthalene diimides as multimodal G-quadruplex-selective ligands. Molecules *24*. https://doi.org/10.3390/molecules24030426.

Platella, C., Trajkovski, M., Doria, F., Freccero, M., Plavec, J., and Montesarchio, D. (2020). On the interaction of an anticancer trisubstituted naphthalene diimide with G-quadruplexes of different topologies: a structural insight. Nucleic Acids Res. 1–14. https://doi.org/10.1093/nar/gkaa1001.

Popov, A., Smirnov, E., Kováčik, L., Raška, O., Hagen, G., Stixová, L., and Raška, I. (2013). Duration of the first steps of the human rRNA processing. Nucleus (United States) *4*, 134–141. https://doi.org/10.4161/nucl.23985.

Răsădean, D.M., Sheng, B., Dash, J., and Pantoş, G.D. (2017). Amino-acid-derived naphthalenediimides as versatile G-quadruplex binders. Chem. A Eur. J. *23*, 8491–8499. https://doi.org/10.1002/chem.201700957.

Siebeneicher, H., Cleve, A., Rehwinkel, H., Neuhaus, R., Heisler, I., Müller, T., Bauser, M., and Buchmann, B. (2016). Identification and optimization of the first highly selective GLUT1 inhibitor BAY-876. ChemMedChem *11*, 2261–2271. https://doi.org/10.1002/cmdc.201600276.

Tawani, A., Mishra, S.K., and Kumar, A. (2017). Structural insight for the recognition of G-quadruplex structure at human c-myc promoter sequence by flavonoid Quercetin. Sci. Rep. *7*, 1–13. https://doi.org/10.1038/s41598-017-03906-3.

Thorens, B., and Mueckler, M. (2010). Glucose transporters in the 21st century. Am. J. Physiol. Endocrinol. Metab. *298*, 141–145. https://doi.org/10.1152/ajpendo.00712.2009.

Todd, A.K., Johnston, M., and Neidle, S. (2005). Highly prevalent putative quadruplex sequence motifs in human DNA. Nucleic Acids Res. *33*, 2901–2907. https://doi.org/10.1093/nar/gki553.

Cuenca, F., Greciano, O., Gunaratnam, M., Haider, S., Munnur, D., Nanjunda, R., Wilson, W.D., and Neidle, S. (2008). Tri- and tetra-substituted naphthalene diimides as potent G-quadruplex ligands. Bioorg. Med. Chem. Lett. *18*, 1668–1673. https://doi.org/10.1016/j.bmcl.2008.01.050.

Wei, T., Najmi, S.M., Liu, H., Peltonen, K., Kucerova, A., Schneider, D.A., and Laiho, M. (2018). 'Small-molecule targeting of RNA polymerase I activates a conserved transcription elongation checkpoint. Cell Rep. *23*, 404–414. https://doi.org/10.1016/j.celrep.2018.03.066.

Xu, H., Di Antonio, M., McKinney, S., Mathew, V., Ho, B., O'Neil, N.J., Dos Santos, N., Silvester, J., Wei, V., Garcia, J., et al. (2017). CX-5461 is a DNA G-quadruplex stabilizer with selective lethality in BRCA1/2 deficient tumours. Nat. Commun. *8*, 14432. https://doi.org/10.1038/ncomms14432.

Yang, J., Wen, J., Tian, T., Lu, Z., Wang, Y., Wang, Z., Wang, X., and Yang, Y. (2017). GLUT-1 overexpression as an unfavorable prognostic biomarker in patients with colorectal cancer. Oncotarget *8*, 11788–11796. https://doi.org/10.18632/oncotarget.14352.

Zhang, S., Sun, H., Chen, H., Li, Q., Guan, A., Wang, L., Shi, Y., Xu, S., Liu, M., and Tang, Y. (2018). Direct visualization of nucleolar G-quadruplexes in live cells by using a fluorescent light-up probe. Biochim. Biophys. Acta *1862*, 1101–1106. https://doi.org/10.1016/j.bbagen.2018.01.022.

Zuffo, M., Stucchi, A., Campos-Salinas, J., Cabello-Donayre, M., Martínez-García, M., Belmonte-Reche, E., Pérez-Victoria, J.M., Mergny, J.L., Freccero, M., Morales, J.C., and Doria, F. (2019). Carbohydrate-naphthalene diimide conjugates as potential antiparasitic drugs: synthesis, evaluation and structure-activity studies. Eur. J. Med. Chem. *163*, 54–66. https://doi.org/10.1016/j.ejmech.2018.11.043.

STAR★METHODS

KEY RESOURCES TABLE

REAGENT or RESOURCE	SOURCE	IDENTIFIER
Antibodies		
Nucleolin	Invitrogen	Cat #39-6400; RRID: AB_2533426
Fibrillarin	Abcam	Cat #ab5821; RRID: AB_2105785
POLR1A	Santa Cruz Biotechnology	Cat #sc-48385; RRID: AB_675814
LC3	MBL	Cat #PD014; RRID: AB_843283
FLAG	Sigma Aldrich	Cat #F1804; RRID: AB_262044
Actin	Sigma Aldrich	Cat #A5441; RRID: AB_476744
Mouse Alexa Fluor 488	Invitrogen	Cat #A-11001; RRID: AB_2534069
Rabbit Alexa Fluor 555	Invitrogen	Cat #A-31572; RRID: AB_162543
Mouse HRP conjugated	Promega	Cat #W4021; RRID: AB_430834
Rabbit HRP conjugated	Promega	Cat #W4011; RRID: AB_430833
Biological samples		
Patient samples	University Hospital Virgen de las Nieves, Granada, Spain	N/A
Chemicals, peptides, and recombinant proteins		
Naphthalene-diimide derivatives	Laboratory of Juan Carlos Morales, CSIC, Granada, Spain. (Zuffo et al., 2019)	N/A
BG4 antibody	Laboratory of Jose Antonio Garcia Salcedo, Genyo, Granada, Spain. (Biffi et al., 2013)	N/A
Critical commercial assays		
Resazurin Fluorimetric Assay	Sigma Aldrich	Cat #R7017
Propidium iodide	Sigma Aldrich	Cat #P4864
Trizol Reagent	Invitrogen	Cat #15596
RevertAid First Strand cDNA Synthesis Kit	Thermo Scientific	Cat #K1622
SYBR Green	Thermo Scientific	Cat #4309155
Pierce Protein A/G Magnetic Beads	Thermo Scientific	Cat #88802
CX5461	MedChemExpress	Cat #HY-13323
BAY876	Sigma-Aldrich	Cat #SML1774
WZB117	Sigma-Aldrich	Cat #400036
TOPRO3	Thermo Scientific	Cat #T3605
Thioflavin T	Sigma-Aldrich	Cat #T3516
Experimental models: Cell lines		
CRL1790 cell line	ATCC	CCD 841 CoN
SW480 cell line	ATCC	SW480 [SW-480]
SW620 cell line	ATCC	SW620 [SW-620]
Oligonucleotides		
Primers for qRTPCR, see Table S1B	Sigma-Aldrich	N/A
G4-oligonucleotides for FID assay, see Table S2	Sigma-Aldrich	N/A
G4_F5 forward oligo for PCR-stop assay: 5'-TCGCGTGGGGG GCGGGTGGTTGGG-3'	Sigma-Aldrich	N/A
G4_F5 reverse oligo for PCR-stop assay: 5'-TTCTCGTCCCAACCAC-3'	Sigma-Aldrich	N/A

(*Continued on next page*)

Continued

REAGENT or RESOURCE	SOURCE	IDENTIFIER
MUT_F5 forward oligo for PCR-stop assay: 5'-TCGCGTCCACTTCAAGTGGTTGGG-3'	Sigma-Aldrich	N/A
G4_F5 oligo for NMR experiments: 5'-TGGGGGGCGGGTGGTTGGGT-3'	Sigma-Aldrich	N/A
Software and algorithms		
FlowJo	BD Biosciences	https://www.flowjo.com/
Fiji	ImageJ	https://imagej.nih.gov/ij/
Oncomine	Thermo Fisher Scientific	https://www.oncomine.org/
Prism	GraphPad	https://www.graphpad.com/scientific-software/prism/
QGRS Mapper	Ramapo College Bioinformatics	http://bioinformatics.ramapo.edu/QGRS/index.php

RESOURCE AVAILABILITY

Lead contact

Further information and request for resources and reagents should be directed to and will be fulfilled by the lead contact, Jose Antonio Garcia-Salcedo (jags@genyo.es).

Materials availability

This study did not generate new unique reagents.

Data and code availability

This study did not generate datasets or codes.

EXPERIMENTAL MODEL AND SUBJECT DETAILS

Cell lines

Cell lines were purchased from American Type Culture Collection and all procedures were carried out under aseptic conditions meeting biological safety requirements. CRL1790 was derived from a female fetus of 21 weeks gestation, SW480 was established from a primary adenocarcinoma of the colon from a 50 year old male donor and SW620 was derived from a metastasis of the same tumor from which the SW480 was derived. Non-tumoral CRL1790 cell line was grown in MEM medium, whereas tumoral SW480 and SW620 cells were maintained in RPMI medium. Both mediums were supplemented with 10% fetal bovine serum, penicillin (5000 U/mL), streptomycin (5 mg/mL) and amphotericin (25 μg/mL). They were cultured at 37°C and 5% CO_2 atmosphere.

Human samples

Samples of patients with CRC were obtained from University Hospital Virgen de las Nieves, Granada, Spain. Informed consent was obtained from all patients included in the study, which was approved by the local Ethical Committee of the University of Granada (Spain). Before treatment, tumor biopsies from 15 patients and histologically non-tumoral adjacent tissue from 7 patients were collected and freshly frozen until RNA extraction. Both female (10) and male (12) donors were included, with a mean age of 59 years old (ranging from 51 to 66 years old). No statistically significant differences were found in terms of developmental stage, age or gender when comparing the two groups (tumoral and non-tumoral).

METHOD DETAILS

NDIs preparation

NDIs previously synthesized in a reported work (Arévalo-Ruiz et al., 2017; Zuffo et al., 2019) were used. Within the huge variety of NDI derivatives available, we selected carbohydrate-conjugated NDIs for our study in an attempt for a targeted antitumoral therapy according to previous results (Arévalo-Ruiz et al., 2017). Briefly, the carbohydrate-NDI conjugates were synthesized via the copper(I)-catalyzed azide alkyne cycloaddition (CuAAC) click reaction using NDI and sugar moieties as the azide and alkyne coupling partners respectively. Reverse phase preparative HPLC purification afforded the compounds in good yields (65-90%). All NDIs were dissolved in dimethyl sulfoxide (DMSO) and stored at -20°C.

Cytotoxic assay

Cytotoxic activity was screened in triplicate using Resazurin Fluorimetric Assay (R7017, Sigma Aldrich), according to the manufacturer's protocol. Cells seeded into 96-well plates ($8 \cdot 10^3$ cells/well) were treated for 48 h with NDI derivatives in concentrations ranging from $2 \cdot 10^{-5}$ μM to 100 μM. A negative control with DMSO was included. Fluorescence was determined using Nanoquant Infinite M200 Pro multi-plate reader (Tecan). IC50 values were determined by non-linear regression with Graphpad (Prism).

Cell cycle analysis

Cell cycle analyses were carried out by flow cytometry with propidium iodide (PI) (P4864, Sigma Aldrich). SW480 cells (10^6) were seeded into 10 cm culture dishes and treated with T1/T5 at IC50 concentration for 24 h or the vehicle (DMSO) control. Cells were then fixed on ice with ice-cold 70% ethanol and stained with 0.04 mg/mL PI and 0.1 mg/mL ribonuclease A (19101, Qiagen). Cell cycle distribution was determined by an analytical DNA flow cytometer (FACSVerse, BD Biosciences) and FlowJo software with DNA instrument settings on low mode.

Immunofluorescence

Cells under different experimental conditions were seeded into 13-mm circular coverslips and placed in 24-well plates. Fixation was performed with 4% (v/v) paraformaldehyde (P6148, Sigma Aldrich) for 10 min at room temperature (RT), permeabilization with 0.1% (v/v) Triton-X100 (T8787, Sigma Aldrich) for 10 min and blocking with 10% bovine serum albumin (A7906, Sigma Aldrich), 0.5% (v/v) Triton-X100 for 30 min at RT. Primary antibodies were subsequently incubated for 1 h at RT and secondary antibodies for 30 min at 4°C in darkness. All coverslips were mounted onto poly-L-lysine slides (J2800AMNZ, Thermo scientific) with Vectashield (H-1200, Vector) including DAPI (4',6-diamidino-2-phenylindole) for nuclear counterstain. Images were acquired through a Confocal Zeiss LSM 710 inverted microscope with a 63x immersion objective. Antibodies used are listed in Supplementary files (Table S1A). In particular, the G4 selective antibody BG4 was expressed and used for immunofluorescence according to standard method (Biffi et al., 2013).

Western blot

Total protein was extracted using RIPA lysis buffer containing 1% PMSF (P7626, Sigma Aldrich) and 1% protease inhibitor cocktail (P8340, Sigma Aldrich). Protein content was loaded on 10% SDS-polyacrylamide gels (1610148, Bio-Rad) for electrophoresis and wet transferred to nitrocellulose membranes (66485, Pall corporation), which were blocked with 5% semi-skimmed milk and incubated overnight at 4°C with primary antibodies. Membranes were then incubated with Horseradish Peroxidase (HRP)-labeled secondary antibodies for 1 h at RT. After incubation with luminol solution (1705060, Bio-Rad), chemiluminiscence signals were measured using Image Quant LAS 4000 (GE Healthcare Life Sciences). Protein levels were quantified by ImageJ. Experiments were performed in biological triplicate. Antibodies used are listed in Supplementary files (Table S1A).

qRT-PCR

Total cellular RNA was isolated from cells under different experimental conditions with Trizol Reagent (15596, Invitrogen). Reverse transcription was performed using RevertAid First Strand cDNA Synthesis Kit (K1622, Thermo Scientific) with random primers according to the manufacturer's protocol. Quantitative PCR was conducted on 7900HT Fast Real-time PCR System (Applied Biosystems) with SYBR Green (4309155, Thermo Scientific), a final concentration of primers at 500 nM and using 1 μL of 100 ng/μL cDNA in 10 μl reaction. Target mRNA levels were normalized in relation to actin (ΔCt) and fold change was determined using the $2^{-\Delta\Delta Ct}$ method. Experiments were conducted in biological triplicate. Primers used for this study are listed in Supplementary files (Table S1B). CX5461 (HY-13323, MedChemExpress) was used as an established control for Pol I inhibition.

Chromatin immunoprecipitation (ChIP)

Chromatin was extracted as previously described (Wei et al., 2018) and sheared to 500–1,000 bp using Bioruptor Plus (Diagenode). 100 μg of sonicated DNA was immunoprecipitated with 5 μg of mouse α-POLR1A (sc-48385, Santa Cruz Biotechnology) and collected with Pierce Protein A/G Magnetic Beads (88802, Thermo Scientific). DNA was purified using phenol:chloroform:isoamyl alcohol (25:24:1) protocol (P2069, Sigma). Experiments were conducted in biological triplicate.

Fluorescence confocal microscopy

Taking advantage of NDIs' strong emission in the red when excited with 594 nm-laser, experimental preparations to assess NDIs intracellular location were performed as previously described (Arévalo-Ruiz et al., 2017). Images were acquired with a confocal microscope and mean nuclear fluorescence intensity was measured using Fiji software (n>50). To allow comparability, instrument settings were equally adjusted across the different cell lines.

Fluorescence spectroscopy

Quantification of cellular uptake in presence of GLUT1 transporter inhibitors such as BAY876 (SML1774, Sigma-Aldrich) and WZB117 (400036, Sigma-Aldrich) was achieved by fluorescence spectroscopy as previously described (Arévalo-Ruiz et al., 2017). Fluorescence intensity was detected with a Nanoquant Infinite M200 Pro multi-plate reader (Tecan) using 485 nm for excitation and 535 nm for emission; experiments were performed in triplicate. Fluorescence values were calculated as follows: %

Fluorescence = A/B·100; where (A) corresponds to the fluorescence determined for each sample and (B) is the fluorescence in the respective inhibitor-free control samples.

G4s prefolding

G4-oligonucleotides listed in Table S2 were purchased from Sigma Aldrich. All of them were dissolved in G4s buffer (10 mM potassium phosphate buffer containing 100 mM potassium chloride at pH 7.0), heated at 95°C for 10 min, slowly cooled to RT and stored at 4°C.

Fluoresecent intercalator displacement (FID) assay

For FID assays, 5 μM TOPRO3 (T3605, Thermo Scientific) was used as a fluorescent intercalator, being saturated with 10 μM prefolded G4s and titrated with T5 in G4s buffer in 96-well plates. TOPRO3 was excited at 642 nm and emission profile was monitored between 650–800 nm with a multi-plate reader. All assays were conducted in triplicate. Fluorescence values were calculated as follows: %Fluorescence = A/B·100; where (A) is the fluorescence value in presence of T5 and (B) corresponds to the fluorescence value in T5-free controls. The affinity was estimated by the DC50 value, which corresponds to the required concentration of T5 to induce a 50% fluorescence decrease. DC50 values were determined by non-linear regression with Prism Graphpad using increasing concentrations of T5 from 0.02 to 100 μM.

PCR-stop assay

PCR-stop assay was performed as previously described (Tawani et al., 2017) using a test oligonucleotide including G4_F5 (5'-TCGCGTGGGGGGCGGGTGGTTGGG-3') and a partially complementary oligonucleotide (5'-TTCTCGTCCCAACCAC-3'). In parallel, a mutant sequence (MUT_F5) incapable of G4 formation due to guanines 7-12 and 14-16 replacement (5'-TCGCGTCCACTTC AAGTGGTTGGG-3') was considered as a negative control. Amplified products were visualized in a 3% agarose gel in 1X TBE and stained with GelGreen (41005, Biotium). Gel images were analyzed using ImageQuant LAS 4000. Three independent reactions were conducted per concentration.

In vitro transcription assay

A DNA template containing the *Saccharomyces cerevisiae* rDNA promoter (-250 to +56 with respect to the transcription start site) fused to a 700 base pair segment of the human rDNA starting at +3412 (containing the G4_F5 sequence) was synthesized (Genscript). This template was amplified by PCR and incorporated into a multi-round *in vitro* transcription assay for RNA Polymerase I. Transcription assays included all purified components (Pol I, core factor, Rrn3, and TBP) and were performed as previously described (Keener et al., 1998; Bedwell et al., 2012). After preinitiation complexes were formed, T5 (or vehicle) was added to final concentrations indicated. Transcription was initiated with substrate NTPs (200 μM ATP, GTP, CTP, 15 μM UTP, and 10 μCi α-^{32}P UTP) and reactions were halted by addition of 1 M ammonium acetate in 95% ethanol. RNA was precipitated, subjected to 5% denaturing polyacrylamide gel electrophoresis, and visualized by phosphorimaging. At least four independent reactions were conducted per concentration. The runoff RNA species were quantified using Quantity one software (BioRad).

Nuclear Magnetic Resonance (NMR) experiment

A DNA oligonucleotide including G4_F5 sequence (5'-TGGGGGGCGGGTGGTTGGGT-3') was resuspended in H_2O/D_2O 9:1 in 25 mM potassium phosphate, pH 7. NMR titrations were performed by adding increasing amounts of T5 to the oligonucleotide solution at 100 μM. Different R ratios = [T5] / [DNA] were considered (R= 0, 1, 2). NMR spectra were acquired in Bruker Avance spectrometer operating at 600 MHz, and processed with Topspin software. Water suppression was achieved by including a WATERGATE module in the pulse sequence prior to acquisition.

Thioflavin T (ThT) competition assay

Cells seeded into 13-mm circular coverslips and placed in 24-well plates ($8\cdot10^4$ cells/well) were non-treated or treated with T5 1 μM for 3 h. Then, cells were fixed for 10 min in cold methanol, rinsed twice with PBS and incubated with 5 μM ThT (T3516, Sigma-Aldrich) for 15 min. Cellular nuclei were counterstained with PI and visualized by confocal microscopy as previously described (Zhang et al., 2018).

QUANTIFICATION AND STATISTICAL ANALYSIS

Statistical analysis was performed using Prism Graphpad software. Statistical significance was assessed using Student's two-tailed t test and two-way ANOVA. Values represent mean ± SD. For all tests, p values below 0.05 were considered significant and expressed as follows: *$p < 0.05$; **$p < 0.01$ and ***$p < 0.001$. The statistical details of experiments can be found in figure legends.